Nanoscale

COMMUNICATION

View Article Online
View Journal

All solution processed low turn-on voltage near infrared LEDs based on core–shell PbS–CdS quantum dots with inverted device structure†

Cite this: DOI: 10.1039/c4nr01975j

Received 11th April 2014
Accepted 1st June 2014

DOI: 10.1039/c4nr01975j

www.rsc.org/nanoscale

Rafael S. Sanchez,[a] Enrico Binetti,‡[b] Jose A. Torre,[a] G. Garcia-Belmonte,[a] Marinella Striccoli[b] and Ivan Mora-Sero*[a]

Colloidal semiconductor quantum dots (QDs) are extraordinarily appealing for the development of light emitting devices (LEDs) due to tunable and pure color emission, brightness and solution processability. This last advantage of the QD-LEDs is even more evident in the field of infrared emission where the devices currently used are prepared by high cost epitaxial techniques. Here we show the fabrication of low cost NIR QD-LEDs based on high quantum yield core–shell PbS–CdS QDs and a novel inverted device structure. Devices are produced using SnO_2:F (FTO) as the conductive transparent contact, nanostructured TiO_2 as the electron transport layer (ETL) and poly-(3-hexylthiophene) P3HT as the hole transport layer (HTL). Despite the roughness of this ETL, the obtained external quantum efficiencies (EQEs) are similar to previously reported values, obtained with regular configuration and more expensive ITO substrates. A turn-on voltage as low as the QD band gap (1.47 eV) is achieved for a large area (1.54 cm^2) and relatively stable QD-LEDs.

Colloidal quantum dots (QDs) present very unique and suitable electro-optical properties, such as wide and tunable absorption and very narrow and intense emission spectra, for the development of optoelectronic devices.[1–3] In addition, they can be dispersed in solvents, thanks to the presence of organic ligands on their surface, and easily processed under room temperature conditions using low-cost techniques. Importantly, a wide variety of parameters such as solubility,[4] mechanical resistance of the films,[5] inter-dot distance,[6] photo-luminescence quantum yield (PL QY)[2,7] or electrical conductivity,[8] among other characteristics, can be controlled by varying the QD surface passivation agents used for the film preparation, which is usually based on the ligand exchange layer-by-layer deposition methodology.

The PL QY of QDs in solution is a crucial parameter to be maximized in order to produce highly efficient electroluminescent devices, since film deposition of QDs typically induces a significant quenching of the luminescence properties through non-radiative recombination pathways, *e.g.* Förster resonant energy transfer (FRET)[9] or Auger recombination,[10,11] among other feasible mechanisms. In this respect, core–shell QDs present some advantages compared to those composed of a single material. On the one hand, they have enhanced luminescence characteristics, due to the efficient surface passivation of the inorganic shell, reaching in some cases values of PL QYs close to 1.[3,12] On the other hand, core–shell or core–multishell QDs show outstanding photochemical and thermal stability, which is a crucial requirement for the fabrication of stable and long-living light emitting devices.[2,7]

Although much effort is being devoted to exploit QDs in LED technology, there are still issues and limitations to be considered and improved: (i) high turn-on voltages; (ii) low device efficiency; (iii) non-negligible parasitic electroluminescence from adjacent layers; (iv) charge accumulation and subsequent loss of light emission due to an inefficient carrier injection into the QDs;[2] and (v) difficulty of preparing large active area devices due to defects and/or inhomogeneities during the deposition process. Therefore, apart from the optimization of the electro-optical properties of the active layers, the selection of the suitable materials, *i.e.* electron- or hole-transport layers, QD linkers and metal contacts, and the use of the proper device configuration play a crucial role on the ultimate performance of the devices.

Furthermore, despite the interest of NIR LEDs for communications, sensing, night vision screens or labeling, a sensible lower amount of research on this topic has been carried out in comparison with LEDs in the visible range.[3,6,13] Here we demonstrate the successful fabrication of NIR QD-LEDs using colloidal NIR emitting core–shell nanocrystals based on metal chalcogenides, which are constituted by a PbS core covered with

[a]*Photovoltaic and Optoelectronic Devices Group, Departament de Física, Universitat Jaume I, 12071 Castelló, Spain. E-mail: sero@uji.es*

[b]*CNR-IPCF Division of Bari, c/o Department of Chemistry, University of Bari, Via Orabona 4, 70126 Bari, Italy*

† Electronic supplementary information (ESI) available. See DOI: 10.1039/c4nr01975j

‡ Present address: Institute for Polymers, Composites and Biomaterials, National Research Council, Via Sommarive, 14 – 38123 Trento, Italy.

a shell of CdS, a wider gap material, see Fig. 1b. Among the lead chalcogenides, PbS has a larger band-gap than PbSe and PbTe, therefore this material does not require ultra-small sized nanocrystals to tune the gap to the NIR spectral region.[14] The CdS shell generates higher PL QYs,[15] while enhancing notably the photochemical[16] and thermal stability.[17] The NIR QD-LEDs are processed completely by solution techniques using a novel inverted configuration, exhibit a very low turn-on voltage without parasitic electroluminescence and high active area devices can be produced.

The core–shell QDs were synthesized by adopting some modifications to the reported procedures.[18,19] The synthetic procedure was divided in two steps. At first, oleic acid capped PbS QDs of 2.3 and 3.0 nm in diameter were synthesized and purified, and, subsequently, an external shell of CdS was grown on their surface by means of a cation exchange methodology, see ESI† for further experimental details. The QDs were exhaustively characterized and, as it is shown in the TEM image (Fig. 1a), the synthetic methodology produces well dispersed round-shaped QDs with good size uniformity. An illustrative scheme of the type I core–shell morphology is shown in Fig. 1b. The formation of the CdS shell induces a notable enhancement of the photoluminescence properties of the QDs due to an efficient surface defect passivation, Fig. 1c.[20] Therefore, the PL QY in solution of the oleate-capped QDs is increased by almost a twenty-fold factor after the CdS shell growth (from 1.1% to 20% for PbS and PbS–CdS in hexane, respectively) and the stability of the QDs in terms of photo-oxidation reactions is enormously enhanced. Besides, a significant hypsochromic shift of the PL peak is observed after the shell growth, Fig. 1c, which is usually ascribed to the reduction of the core diameter due to the Pb to Cd cation exchange.[21] Type I core–shell QD configuration provokes the localization of the electrons and hole wavefunctions at the core of the nanocrystals, thus favoring the radiative recombination of the charge carriers.[18] Consequently, the excited state dynamics are strongly influenced by the presence of the CdS shell. Fig. 1d shows the time-resolved PL decays of PbS and PbS–CdS QDs in which the core–shell QDs demonstrate a slower decay kinetics (average lifetime of 424 ns for PbS QDs *vs.* 742 ns for core–shell), due to suppression of non-radiative decay processes arising from an effective passivation of the surface defects, see ESI1.†[,22]

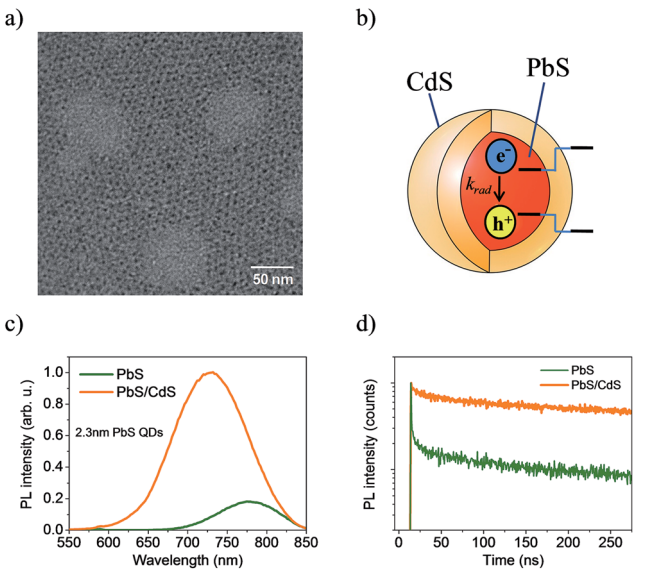

Fig. 1 Characterization of the PbS and PbS–CdS nanocrystals. (a) TEM image of PbS–CdS QDs 3.0 nm in diameter. (b) Schematic structure and relative energy levels of the core–shell QD. (c) Emission spectra of PbS and PbS–CdS QDs (2.3 nm in diameter) under excitation light at 500 nm. (d) Time-resolved PL decay of PbS and PbS–CdS QDs (2.3 nm in diameter), excited with a 200 ps laser source at 375 nm.

With the aim of preparing NIR QD-LEDs, we propose a nanostructured TiO_2 electrode as an electron-transport material (ETM), due to the suitable energy level alignment with PbS nanocrystals[23] and its high refractive index ($n_{TiO_2} = 2.7$),[24] both properties that contribute in the enhancement of the charge injection and light extraction from the devices, respectively.[21,25] In fact higher efficiencies have been obtained if a TiO_2 mesoporous layer is used instead of just a TiO_2 compact layer, probably due to an enhancement of light coupling out efficiency. In addition, TiO_2 films can be easily prepared and show high mechanical, chemical and photochemical stability. The high chemical stability ensures a perfect compatibility with acidic molecules (as thioglycolic acid (TGA), 3-mercaptopropionic acid (MPA)) to perform the ligand exchange of QDs. The inverted device configuration is exploited, as it allows the use of cost efficient TiO_2 and the deposition of the hole transport material (HTM) on the top of the QD layer, thus avoiding its degradation or desorption during the deposition of the QD film.[2] Note that the use of TiO_2 requires annealing at 450 °C, see ESI.† At such a temperature the ITO film changes its optoelectronic properties, which is noticeable from the darkening of the color and a significant decrease of the conductivity, being necessary the use of an alternative transparent conducting oxide as FTO.

A photograph of a working QD-LED and a schematic of the device structure correlated with the cross-sectional scanning electron microscopy (SEM) is shown in Fig. 2a. These devices consist of a patterned FTO cathode, sensibly less expensive than the conventional ITO, a 100 nm TiO_2 blocking layer, a 500 nm nanostructured TiO_2 layer as the ETM, a 250 nm QD layer as the emissive layer, a thin layer of poly(3-hexylthiophene) P3HT as the HTM and a 60 nm gold layer as the anode, see Fig. 2a. The energy-dispersive X-ray analysis (EDX) of the device is shown in the ESI (Fig. S2†). The structure of our devices was designed to achieve efficient charge injection into the core–shell QDs promoted by applying a very low external potential, since the conduction band (CB) and valence band (VB) of PbS match, in terms of energy level alignment, the utilization of TiO_2 as the ETM, P3HT as the HTM and gold as the back contact.[26] In addition, this configuration allows for an all-solution process with cost effective precursors.

The PL of QD layers and the ultimate performance of the devices have been studied by using different linkers, depending on the length of the alkyl chain and the nature of their functional groups, see Fig. 2c. A series of bi-functional organic linkers has been employed for the QD layer assembly, including

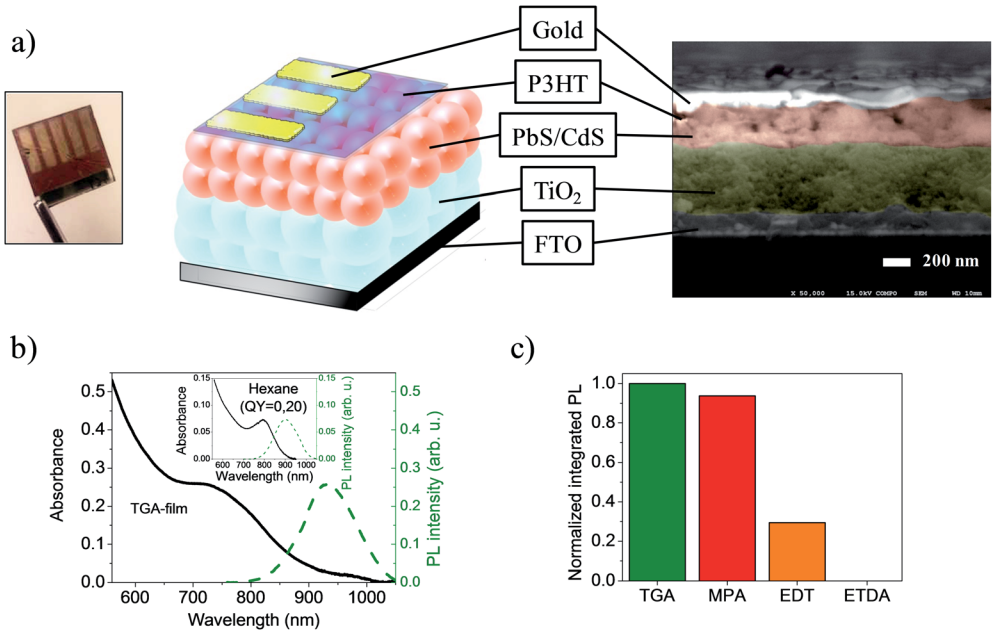

Fig. 2 Structural design of the QD-LEDs. (a) Photograph of a five working contact QD-LED device and the schematic structural configuration of a device showing the different layers of materials correlated with a cross-section SEM image. (b) Absorption and PL spectra of the PbS–CdS QDs in solution (inset) and as QD film using TGA as the linker. The PL QY value was measured in hexane ($\lambda_{exc} = 650$ nm) by the comparative method using the dye IR125 as the emission reference (PL QY = 4.3% in methanol). (c) Integrated photoluminescence intensity of the PbS–CdS QD (3.0 nm in diameter) films ($\lambda_{exc} = 532$ nm) deposited using the corresponding capping agents (TGA, MPA, EDT and ETDA).

TGA, MPA, 1,2-ethanedithiol (EDT) and ethylenediamine (ETDA). EDT and ETDA quenched partially or completely the fluorescence of the QD films, since thiol and amine groups act as hole traps.[27,28] In contrast, the QD films grown with TGA and MPA as capping agents showed high photoluminescence characteristics. The TGA films and devices were taken as references for optimizing the different parameters in this study. Fig. 2b shows the absorption and PL spectra of the 3 nm PbS–CdS nanocrystals in solution (inset) and deposited on a film using TGA as the linker. The optical band-gap (E_g) of the QDs in solution (hexane) was estimated to be 1.47 ± 0.02 eV from the intersection wavelength value between the normalized absorption and emission spectra. It is observed that the Stoke's shift, *i.e.* the energetic difference between the positions of the band maxima of the absorption and emission spectra, is increased from 0.19 eV to approximately 0.32 eV after the film deposition, what could be ascribed to the energy relaxation processes *via* phonon emission and/or to the generation of defects, probably, arising from the ligand exchange and nanocrystal assembly.[29–31] This observation, together with the larger inter-dot interaction after the growth of the QD film, is consistent with red-shift of the emission spectra of QDs ($\Delta\lambda_{em} \approx 30$ nm) after the deposition using TGA as the linker, which may contribute to lower significantly the light emissive properties of the QDs in the film.

Fig. 3a shows the dependence of the radiance spectra of the TGA based device with the increasing potential in the range comprised between 0 and +5 V. The electroluminescence spectra are situated at the same spectral position and present exactly the same shape than PL measurements, see ESI (Fig. S3†), which indicates the absence of parasitic electroluminescence in the ETM or HTM layers. The results indicate that charge carriers are directly injected into the QD layer and undergo subsequent radiative recombination, thus avoiding the exciton generation on the polymer and subsequent energy transfer to the nanocrystals. All the devices prepared using EDT and ETDA for the QD film growth did not show any electroluminescence signal at the studied potential range. This observation is in good agreement with the low PL properties of these films, Fig. 2c. The electroluminescence intensity of the TGA and MPA samples is shown in Fig. 3b, and they exhibit turn-on voltages as low as the QD band-gap, indicating a null potential barrier for electron and hole injection into the PbS–CdS QDs. This result is especially significant taking into account the roughness of the cathode (FTO and mesoporous TiO_2). QD-LEDs present a good rectifying behavior, see Fig. 3c. The Root Mean Square (RMS) roughness of commercial ITO is around 2.5 nm,[32] while the RMS of FTO is one order of magnitude higher.[33] The length of the alkyl chain of the ligands has a significant effect on the electrical properties of the QD films.[6] Shorter hydrocarbon chains give rise to higher current densities. However, the external quantum efficiency values (EQEs), *i.e.* the ratio between the emitted photons and the electrons flowing through a device, were increased significantly for the longer alkyl chain capping agents, see Fig. 3d.[6] It worth mentioning that the EQEs obtained for the MPA based devices are similar to those reported in a previous work using also MPA-ligand PbS QDs and exploiting the direct device configuration on ITO substrates, see Fig. 3d.[6] Devices with a surface area as large as 1.54 cm^2 have been prepared with just a 4-fold decrease of the EQE despite the area being enlarged 7 times, compared to

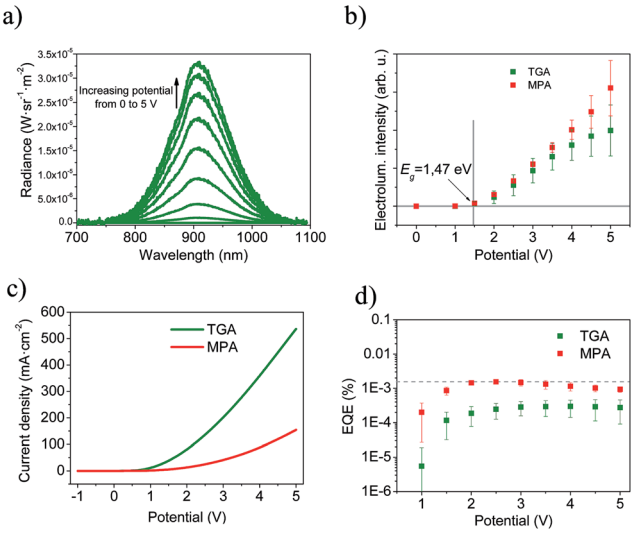

Fig. 3 Opto-electronic characterization of QD-LEDs. (a) Radiance spectra of the TGA based device at different applied potentials (from 0 to +5 V). (b) Electroluminescence intensity of the samples prepared with TGA and MPA as capping agents. The turn-on potentials were calculated from the linear fitting of the electroluminescence intensity values by means of an extrapolation towards the abscissa edge. (c) *J*/*V* curves of the TGA and MPA devices from −1 V to +5 V. PbS–CdS QDs (3.0 nm in diameter). (d) External quantum efficiency (EQE) of the TGA and MPA based devices at the different applied bias. The error bars shown in the graphs (b) and (d) indicate the standard deviation at each potential arising from the measurement of five different devices for TGA and MPA, respectively. The grey dashed line indicates the average EQE obtained in a previous work in the literature for PbS QD-LEDs with MPA in conventional configuration.[6] Note that this information is just included as a reference value as it is not straightforward to compare directly core QDs and core–shell QDs of different sizes.

the devices with the active area of 0.224 cm^2, Fig. 3d. In addition, the response time and the light out-put angle of the devices have been measured (t = 2.3 ms and Ω = 1.47 rad, respectively), see ESI (Fig. S4 and S5†) for further details.

Finally, the stability issues of the QD-LEDs have been analyzed. The prepared devices present a surprising good stability, with intermittent use, during months and stored under air conditions. Under continuous use, the stability is limited due to an electroluminescence drop. The use of the HTM did not have any significant impact on the electroluminescence intensity, turn-on voltage or EQE values, but increased dramatically the lifetime of the devices, see ESI (Fig. S6†). Therefore, the P3HT is supposed to favor the charge extraction from the QD layer. At constant applied bias (3 V) under air atmosphere conditions and without encapsulation, almost the 50% of the initial electroluminescence was preserved after 10 hours of operation, see Fig. 4. It is interesting to see that the decay of electroluminescence correlates with the decay observed in current, pointing out to a decrease of the emission due to a current decrease instead of QD degradation, as stability under intermittent use corroborates. This fact suggests that further optimization of the QD-LED can be achieved by using different HTL and/or deposition processes, which is clearly compatible with the inverse configuration of our devices. The current

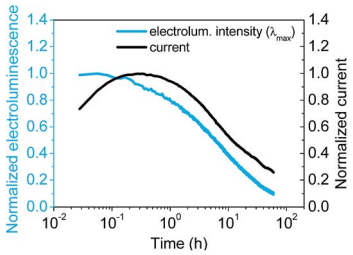

Fig. 4 Operational lifetime. Electroluminescence intensity at the λ_{max} and electric current monitoring of the device during 60 hours under continuous operation. Measurement carried out at continuous applied bias of 3 V under air atmosphere conditions and without encapsulation.

decrease over the time is probably due to charge trapping at the bulk QD film and it is under current study.

In summary, all solution processed NIR QD-LEDs with inverse configuration based on highly luminescent core–shell PbS–CdS QDs have been produced. The PbS–CdS QDs are characterized by tunable and intense PL, high photostability and solution processability. Low cost FTO and TiO_2 layer has been used as the ETL, instead of the conventional ITO. Despite the roughness of the ETL, the measured EQE with the MPA linker is similar to the previously reported values with direct configuration and ITO substrate. In addition, our methodology allows the preparation of large active area devices with a turn-on potential as low as the QD band gap, and presents excellent lifetime (months) under intermittent use and a relatively limited performance under continuous use (50% electroluminescence drop after 10 hours). We do believe that the efficiency obtained with this new configuration can be even enhanced specially by using an alternative HTL. The use of a wide variety of HTL and deposition methods is reachable by exploiting the inverse configuration.

Acknowledgements

This work was partially supported by Generalitat Valenciana (ISIC/2012/008), and FP7 European project ORION (Large CP-IP 229036-2), and Universitat Jaume I project 12I361.01/1. We thank SCIC from Universitat Jaume I for the help with SEM measurements, and R. Comparelli from CNR IPCF for TEM measurements. The financial support from the Research Project PON R&C 2007-2013 MAAT "Molecular Nanotechnology for Health and Environment" (PON 02_00563_3316357) is gratefully acknowledged.

References

1 K.-S. Cho, E. K. Lee, W.-J. Joo, E. Jang, T.-H. Kim, S. J. Lee, S.-J. Kwon, J. Y. Han, B.-K. Kim, B. L. Choi and J. M. Kim, *Nat. Photonics*, 2009, **3**, 341–345.

2 J. Kwak, W. K. Bae, D. Lee, I. Park, J. Lim, M. Park, H. Cho, H. Woo, D. Y. Yoon, K. Char, S. Lee and C. Lee, *Nano Lett.*, 2012, **12**, 2362–2366.

3 Y. Shirasaki, G. J. Supran, M. G. Bawendi and V. Bulovic, *Nat. Photonics*, 2013, **7**, 13–23.
4 F. Dubois, B. Mahler, B. Dubertret, E. Doris and C. Mioskowski, *J. Am. Chem. Soc.*, 2006, **129**, 482–483.
5 L. Zhou, C. Gao and W. Xu, *J. Mater. Chem.*, 2010, **20**, 5675–5681.
6 L. Sun, J. J. Choi, D. Stachnik, A. C. Bartnik, B.-R. Hyun, G. G. Malliaras, T. Hanrath and F. W. Wise, *Nat. Nanotechnol.*, 2012, **7**, 369–373.
7 X. Wang, W. Li and K. Sun, *J. Mater. Chem.*, 2011, **21**, 8558–8565.
8 G. D. Lilly, A. C. Whalley, S. Grunder, C. Valente, M. T. Frederick, J. F. Stoddart and E. A. Weiss, *J. Mater. Chem.*, 2011, **21**, 11492–11497.
9 T.-W. F. Chang, A. Maria, P. W. Cyr, V. Sukhovatkin, L. Levina and E. H. Sargent, *Synth. Met.*, 2005, **148**, 257–261.
10 W. K. Bae, Y.-S. Park, J. Lim, D. Lee, L. A. Padilha, H. McDaniel, I. Robel, C. Lee, J. M. Pietryga and V. I. Klimov, *Nat. Commun.*, 2013, **4**, 2661.
11 D. Bozyigit, O. Yarema and V. Wood, *Adv. Funct. Mater.*, 2013, **23**, 3024–3029.
12 J. M. Pietryga, D. J. Werder, D. J. Williams, J. L. Casson, R. D. Schaller, V. I. Klimov and J. A. Hollingsworth, *J. Am. Chem. Soc.*, 2008, **130**, 4879–4885.
13 M. Stevenson, J. Kamplain, J. Perkins, Z. Zhou, M. Bunda, S. Coe-Sullivan, J. S. Steckel and P. Kazlas, *IR quantum dots for defense applications*, 2013.
14 L. Bakueva, S. Musikhin, M. A. Hines, T.-W. F. Chang, M. Tzolov, G. D. Scholes and E. H. Sargent, *Appl. Phys. Lett.*, 2003, **82**, 2895–2897.
15 O. Chen, J. Zhao, V. P. Chauhan, J. Cui, C. Wong, D. K. Harris, H. Wei, H.-S. Han, D. Fukumura, R. K. Jain and M. G. Bawendi, *Nat. Mater.*, 2013, **12**, 445–451.
16 H.-J. Zhan, P.-J. Zhou, R. Ma, X.-J. Liu, Y.-N. He and C.-Y. Zhou, *J. Fluoresc.*, 2013, 1–9.
17 W. Guo, J. J. Li, Y. A. Wang and X. Peng, *J. Am. Chem. Soc.*, 2003, **125**, 3901–3909.
18 M. V. Kovalenko, R. D. Schaller, D. Jarzab, M. A. Loi and D. V. Talapin, *J. Am. Chem. Soc.*, 2012, **134**, 2457–2460.
19 M. S. Neo, N. Venkatram, G. S. Li, W. S. Chin and W. Ji, *J. Chem. Phys. C*, 2010, **114**, 18037–18044.
20 M. S. de la Fuente, R. S. Sánchez, V. González-Pedro, P. P. Boix, S. G. Mhaisalkar, M. E. Rincón, J. Bisquert and I. Mora-Seró, *J. Chem. Phys. Lett.*, 2013, **4**, 1519–1525.
21 P. Reiss, M. Protière and L. Li, *Small*, 2009, **5**, 154–168.
22 M. J. Fernée, A. Watt, J. Warner, S. Cooper, N. Heckenberg and H. Rubinsztein-Dunlop, *Nanotechnology*, 2003, **14**, 991.
23 B.-R. Hyun, Y.-W. Zhong, A. C. Bartnik, L. Sun, H. D. Abruña, F. W. Wise, J. D. Goodreau, J. R. Matthews, T. M. Leslie and N. F. Borrelli, *ACS Nano*, 2008, **2**, 2206–2212.
24 F. W. Mont, J. K. Kim, M. F. Schubert, E. F. Schubert and R. W. Siegel, *J. Appl. Phys.*, 2008, **103**, 083120.
25 T. Tsutsui, M. Yahiro, H. Yokogawa, K. Kawano and M. Yokoyama, *Adv. Mater.*, 2001, **13**, 1149–1152.
26 S. H. Im, H.-J. Kim, S. W. Kim, S.-W. Kimb and S. I. Seok, *Energy Environ. Sci.*, 2011, **4**, 4181–4186.
27 A. A. Cordones and S. R. Leone, *Chem. Soc. Rev.*, 2013, **42**, 3209–3221.
28 S. Jeong, M. Achermann, J. Nanda, S. Ivanov, V. I. Klimov and J. A. Hollingsworth, *J. Am. Chem. Soc.*, 2005, **127**, 10126–10127.
29 N. O. Dantas, P. M. N. de Paula, R. S. Silva, V. López-Richard and G. E. Marques, *J. Appl. Phys.*, 2011, **109**, 024308.
30 M. J. Fernée, E. Thomsen, P. Jensen and H. Rubinsztein-Dunlop, *Nanotechnology*, 2006, **17**, 956.
31 J. H. Warner, E. Thomsen, A. R. Watt, N. R. Heckenberg and H. Rubinsztein-Dunlop, *Nanotechnology*, 2005, **16**, 175.
32 Y. Yang, Q. Huang, A. W. Metz, J. Ni, S. Jin, T. J. Marks, M. E. Madsen, A. DiVenere and S. T. Ho, *Adv. Mater.*, 2004, **16**, 321–324.
33 T.-H. Fang and W.-J. Chang, *Appl. Surf. Sci.*, 2003, **220**, 175–180.